J|A|C|S
ARTICLES
Published on Web 03/15/2007

Protein Phosphorylation and Intermolecular Electron Transfer: A Joint Experimental and Computational Study of a Hormone Biosynthesis Pathway

Andy Zöllner,[†] Melissa A. Pasquinelli,*[,‡,§] Rita Bernhardt,[†] and David N. Beratan[‡]

Contribution from the Universität des Saarlandes, 66123 Saarbrücken, Germany, and Department of Chemistry, Duke University, Durham, North Carolina 27708

Received July 6, 2006; E-mail: Melissa_Pasquinelli@ncsu.edu

Abstract: Protein phosphorylation is a common regulator of enzyme activity. Chemical modification of a protein surface, including phosphorylation, could alter the function of biological electron-transfer reactions. However, the sensitivity of intermolecular electron-transfer kinetics to post-translational protein modifications has not been widely investigated. We have therefore combined experimental and computational studies to assess the potential role of phosphorylation in electron-transfer reactions. We investigated the steroid hydroxylating system from bovine adrenal glands, which consists of adrenodoxin (Adx), adrenodoxin reductase (AdR), and a cytochrome P450, CYP11A1. We focused on the phosphorylation of Adx at Thr-71, since this residue is located in the acidic interaction domain of Adx, and a recent study has demonstrated that this residue is phosphorylated by casein kinase 2 (CK2) in vitro.[1] Optical biosensor experiments indicate that the presence of this phosphorylation slightly increases the binding affinity of oxidized Adx with $CYP11A1_{ox}$ but not AdR_{ox}. This tendency was confirmed by K_A values extracted from Adx concentration-dependent stopped-flow experiments that characterize the interaction between AdR_{red} and Adx_{ox} or between Adx_{red} and $CYP11A1_{ox}$. In addition, acceleration of the electron-transfer kinetics measured with stopped-flow is seen only for the phosphorylated Adx−CYP11A1 reaction. Biphasic reaction kinetics are observed only when Adx is phosphorylated at Thr-71, and the Brownian dynamics (BD) simulations suggest that this phosphorylation may enhance the formation of a secondary Adx−CYP11A1 binding complex that provides an additional electron-transfer pathway with enhanced coupling.

Introduction

Much of biological electron transfer (ET) occurs between proteins.[2−4] As such, these molecular processes involve molecular recognition as well as nonadiabatic electron transfer. The rate constants may be limited by recognition docking (diffusion or gating limit) or by thermally activated electron tunneling (ET or activation limit).[5,6] The structure of protein surfaces, critical for recognition and docking, is often changed by post-translational modification, and these changes could alter the function of biological electron-transfer chains.

Because of the extensive role of electron transport reactions in the cell, it can be imagined that switches and control mechanisms for these reactions could direct electrons to the proper location, in the appropriate numbers, and at the necessary times.[7,12] Indeed, oxidation (or reduction) at the wrong time may prove to be lethal. There are many signaling and switching mechanisms available to proteins.[9] A common regulatory signal for enzyme activity is phosphorylation, which is performed by protein kinases. However, whether protein phosphorylation affects intermolecular electron transfer has not been thoroughly investigated. We have therefore combined experimental and computational studies to assess the potential role of post-translational modifications in electron-transfer chains.

Kinetic control of intramolecular electron transfer is relatively well understood. Marcus theory describes the reaction free energy dependence of the reaction rates,[10] and tunneling pathway theories[11] describe the dependence of the donor−acceptor

[†] Universität des Saarlandes.
[‡] Duke University.
[§] Present address: Fiber and Polymer Science Program, Department of Textile Engineering, Chemistry, and Science, North Carolina State University, Raleigh, NC 27695.

(1) Bureik, M.; Zöllner, A.; Schuster, N.; Montenarh, M.; Bernhardt, R. *Biochemistry* **2005**, *44*, 3821−3830.
(2) Bendall, D. S., Ed. *Protein Electron Transfer*; Bios Scientific Publishers: Oxford, 1996.
(3) Kuznetsov, A. M.; Ulstrup, J. *Electron Transfer in Chemistry and Biology;* Wiley: Chichester, 1999.
(4) Balzani, V., Ed. *Electron Transfer in Chemistry, Vols. 1−4*; Wiley-VCH: New York, 2001.
(5) Pilling, M. J.; Seakins, P. W. *Reaction Kinetics*; Oxford University Press: Oxford, 1995; pp 144−146.
(6) Davidson, V. L. *Acc. Chem. Res*. **2000**, *33*, 87−93.
(7) Schuster, G. B., ed. *Topics in Current Chemistry, Vols. 236−237*; Springer: New York, 2004.
(8) Yavin, E.; Boal, A. K.; Stemp, E. D. A.; Boon, E. M.; Livingston, A. L.; O'Shea, V. L.; David, S. S.; Barton, J. K. *Proc. Natl. Acad. Sci. U.S.A.* **2005**, *102*, 3546−3558.
(9) Helmreich, E. J. M. *The Biochemistry of Cell Signaling*; Oxford Press: New York, 2001.
(10) Marcus, R. A.; Sutin, N. *Biochim. Biophys. Acta* **1985**, *811*, 265−322.
(11) (a) Beratan, D. N.; Onuchic, J. N.; Winkler, J. R.; Gray, H. B. *Science* **1992**, *258*, 1740−1741. (b) Onuchic, J. N.; Beratan, D. N.; Winkler, J. R.; Gray, H. B. *Annu. Rev. Biophys. Biomol. Struct.* **1992**, *21*, 349−377. (c) Skourtis, S. S.; Beratan, D. N. *Adv. Chem. Phys.* **1999**, *106*, 377−452.
(12) (a) Gray, H. B.; Winkler, J. R. *Q. Rev. Biophys.* **2003**, *36*, 341−372. (b) Prytkova, T. R.; Kurnikov, I. V.; Beratan, D. N. *Science* **2007**, *312*, 622−625.

10.1021/ja064803j CCC: $37.00

interaction on the three-dimensional protein structure. Experimental studies of chemically labeled proteins, especially ruthenium-modified proteins, have mapped out the structure dependence of these rate constants in solution.[12] Moreover, recent experiments with these proteins in crystal lattices have explored interprotein ET rates in known geometries.[12]

Interprotein interactions combine electrostatic and hydrophobic forces, including structural rearrangements at the interface. Recent studies of protein−protein electron transfer in solution[13,14] and in chemically linked protein−protein structures[13,14] suggest that geometries that are electron-transfer active can comprise a minority of the ensemble of docked protein structures. In the case of electrostatic docking, changes in charged groups near the redox cofactors can alter the ET rate by orders of magnitude.[15] Interestingly, these large rate enhancements need not be accompanied by changes in binding constants, suggesting that changes in the population of a minority of "active" species may control the interprotein ET kinetics. For instance, in studies of myoglobin-cytochrome b_5 electron transfer, changes in the myoglobin charge by −1 near the cofactor interface slowed the ET rate 10-fold, while increasing the charge by +1 enhanced the rate by about 10-fold, and neither charge mutation had a significant impact on the binding constant. We hypothesize that similar changes in ET kinetics may accompany protein surface phosphorylation.

Since it has long been hypothesized that control of ET by phosphorylation plays a role in vitamin D metabolism and in steroid biosynthesis,[16,17] we have focused our studies on the mitochondrial steroid hydroxylating system from bovine adrenal glands. This electron-transfer system consists of a [2Fe−2S] ferredoxin (adrenodoxin, Adx), an FAD containing ferredoxin reductase (adrenodoxin reductase, AdR), and a cytochrome P450.[18] The electrons are supplied to AdR via NADPH, and then Adx shuttles the electrons from AdR to a membrane-bound cytochrome P450 that uses the electrons for subsequent substrate hydroxylation. For instance, bovine Adx participates in the biosynthesis of steroid hormones by mediating the electron transport to the heme iron of two steroid hydroxylating cytochromes P450, cytochrome $P450_{SCC}$ (or CYP11A1) and $P450_{11\beta}$ (or CYP11B1), which are localized in the inner mitochondrial membrane of the adrenal cortex. The first and rate-limiting step in the synthesis of steroid hormones, the formation of pregnenolone from cholesterol, is catalyzed by CYP11A1,[19] whereas CYP11B1 hydroxylates 11-deoxycorticosterone and 11-deoxycortisol to form the products, corticosterone, 18-OH-corticosterone, aldosterone, and cortisol, respectively.[20] The recognition of Adx with its redox partners depends mainly on electrostatic interactions involving an acidic interaction domain of Adx from residues 67 to 87.[21,22] Additional sites involved in redox partner binding on the core domain have been identified in the crystal structure of a crosslinked 1:1 complex of Adx and AdR[23] and by site-directed mutagenesis studies.[24,27] These newly discovered interaction sites comprise a second acidic patch around position Asp-39, the loop surrounding the iron-sulfur cluster,[24,27] and involve C-terminal residues of the ferredoxin.[25]

Recent investigations[1] have shown that Adx is phosphorylated in vitro at position T71 by casein kinase 2 (CK2). This kinase is a ubiquitous Ser and Thr phosphorylating enzyme that possesses a very simple phosphorylation motif ([S/T]−X−X−[D/E]).[26,27] Since the presence of CK2 in the mitochondria has been demonstrated,[28] phosphorylation of components of the mitochondrial steroid hydroxylating ET chain by CK2 could influence the ET. In fact, it was shown that CK2 phosphorylated Adx and a mutant that simulates phosphorylation at residue 71, Adx-T71E, both led to an enhanced formation of pregnenolone from cholesterol as measured in an in vitro reconstituted CYP11A1 system (approximately 1.5-fold).[1] However, these observed changes could be caused by an enhanced binding between these Adx mutants and CYP11A1 or by the ET event itself. Moreover, these Adx surface residue changes could also affect the interaction with its other redox partner, AdR.

Here, we study the influence of phosphorylations on intermolecular ET reactions. Surface plasmon resonance experiments were used as a first test to determine whether the association constants between Adx and its redox partners, both in their oxidized state, were altered by phosphorylation. Additionally, in order to characterize the binding between the physiologically relevant redox states (AdR_{red}−Adx_{ox} and Adx_{red}−$CYP11A1_{ox}$), we extracted K_A values from stopped-flow experiments that were also used to analyze possible changes in the electron-transfer rates of the different Adx forms. These biochemical data for the interaction between Adx and CYP11A1 were complemented with Brownian dynamics (BD) calculations. The results of this study suggest that protein phosphorylations can directly influence ET kinetics. Both the experimental and theoretical results indicate that phosphorylation of Adx at residue Thr 71 somewhat increases the bimolecular rate of ET with CYP11A1 but not AdR and that the phophorylated protein may employ an alternate protein−protein conformation for the ET event compared to the unmodified form.

Experimental Methods

Mutagenesis, Expression, and Enzyme Purification. All Adx proteins were produced in the host *E. coli* BL21 (DE3) pLysE using

(13) (a) Van Amsterdam, I. M. C.; Ubbink, M.; Einsle, O.; Messerschmidt, A.; Merli, A.; Cavazzini, D.; Rossi, G. L.; Canters, G. W. *Nat. Struct. Biol.* **2002**, *9*, 48−52. (b) Lin, J.; Balabin, I. A.; Beratan, D. N. *Science* **2005**, *310*, 1311−1313.
(14) Willner, I.; Katz, E., Eds. *Bioelectronics*; Wiley-VCH: Weinheim, 2005.
(15) (a) Zhao-Xun; Kurnikov, I. V.; Nocek, J. M.; Mauk, A. G.; Beratan, D. N.; Hoffman, B. M. *J. Am. Chem. Soc.* **2004**, *126*, 2785−2798. (b) Liang, Z. X.; Nocek, J. M.; Huang, K.; Hayes, R. T.; Kurnikov, I. V.; Beratan, D. N.; Hoffman, B. M. *J. Am. Chem. Soc.* **2002**, *124*, 6849−6859.
(16) Jones, G.; Strugnell, S. A.; DeLuca, H. F. *Physiol. Rev.* **1998**, *78*, 1193−1223.
(17) Monnier, N.; Defaye, G.; Chambaz, E. M. *Eur. J. Biochem.* **1987**, *169*, 147−153.
(18) (a) Bernhardt, R. *Curr. Opin. Endocrin. Diab.* **2000**, *7*, 109−115. (b) Bernhardt, R. *Rev. Physiol. Biochem. Pharmacol.* **1996**, *127*, 137−221.
(19) Lambeth, J. D. In *Frontiers in Biotransformation*; Ruckpaul, K., Rein, H., Eds.; Akademie-Verlag: Berlin, 1990; pp 58−100.
(20) Bureik, M.; Lisurek, M.; Bernhardt, R. *Biol. Chem.* **2002**, *383*, 1537−1551.
(21) Vickery, L. E. *Steroids* **1997**, *62*, 124−127.
(22) Grinberg, A. V.; Hannemann, F.; Schiffler, B.; Muller, J.; Heinemann, U.; Bernhardt, R. *Proteins* **2000**, *40*, 590−612.
(23) Muller, E. C.; Lapko, A.; Otto, A.; Muller, J. J.; Ruckpaul, K.; Heinemann, U. *Eur. J. Biochem.* **2001**, *268*, 1837−1843.
(24) Zollner, A.; Hannemann, F.; Lisurek, M.; Bernhardt, R. *J. Inorg. Biochem.* **2002**, *91*, 644−654.
(25) Uhlman, H.; Kraft, R.; Bernhardt, R. *J. Biol. Chem.* **1994**, *269*, 22557−22564.
(26) (a) Litchfield, D. W. *Biochem. J.* **2003**, *369*, 1−15. (b) Meggio, F.; Brunati, A. M.; Donella-Deana, A.; Pinna, L. A. *Eur. J. Biochem.* **1984**, *138*, 379−385.
(27) Hannemann, F.; Rottmann, M.; Schiffler, B.; Zapp, J.; Bernhardt, R. *J. Biol. Chem.* **2001**, *276*, 1369−1375.
(28) Faust, M.; Montenarh, M. *Cell Tissue Res.* **2000**, *301*, 329−340.

the plasmid pET3d[29] bearing the cDNA for each Adx mutant or Adx wild type (WT-Adx).[27,30] Amino acid substitutions were generated with the QuikChange site directed mutagenesis kit (Stratagene; La Jolla, CA). Oligonucleotides containing the appropriate mutations were synthesized by BioTez GmbH (BioTez; Berlin, Germany). Recombinant Adx, Adx mutants, and AdR were purified as described elsewhere.[30,31] Protein concentrations were calculated using $\epsilon_{414} = 9.8$ (mM cm)$^{-1}$ for Adx[32] and $\epsilon_{450} = 11.3$ (mM cm)$^{-1}$ for AdR.[33] CYP11A1 was isolated from bovine adrenal glands using the protocol of Akhrem et al.[34] with minor modifications. Human CK2 holoenzyme was kindly made available by the group of Prof. Montenarh, Uni-Klinik Homburg.[35]

In Vitro Phosphorylation by Protein Kinase CK2. Phosphorylation reactions were carried out at 37 °C and in a total volume of 300 μL (50 mM Tris-HCl at pH 7.5, 100 mM NaCl, 10 mM $MgCl_2$, 1 mM DTT, 70 μM Adx (302 μg Adx), 15 μg of CK2, and 250 μM ATP). Samples were incubated for 2 h and then diluted in the buffer required for each experiment. Prior to using each sample, the degree of phosphorylated Adx was measured by quantifying the amount of ATP remaining in the solution after the kinase reaction had taken place. ATP consumption was determined with the Kinase-GloTM luminescent kit (V6711, Promega; Madison, WI) following the supplied instructions. After the phoshorylation reaction took place, samples were diluted in PBS buffer (pH 7.5) 250-fold. Then 100 μL of the diluted sample were loaded onto a solid white 96 well plate (Nunc; Wiesbaden, Germany) and supplemented with 100 μL of luminescent reagent. After 10 min of incubation at room temperature, the luminescent signal was recorded on a Genios reader (TECAN; Groedig, Austria), with an integration time of 150 ms and the signal gain set to 100.

Optical Biosensor Measurements. Formation of the Adx_{ox}/$CYP11A1_{ox}$ or Adx_{ox}/AdR_{ox} complex was assayed on a Biacore 2000 system using CM5 chips with a carboxymethylated dextran surface as previously published.[24,36] Activation of the chip was achieved by two injections of 50 μL of a 1-ethyl-3-(3-dimethylaminopropyl)carbodiimide (EDC) and *N*-hydroxysuccinimide (NHS) mixture. Free amino groups of the ferredoxin, which are distributed equally on the protein surface, were used in order to randomly attach the protein to the EDC/NHS activated carboxyl groups of the sensor chip dextran matrix. Since positively charged free amino groups in Adx do not directly participate in the redox partner binding and recognition, this coupling procedure will not hinder the correct interaction between Adx and its redox partners. Nevertheless, it cannot be excluded that some of the Adx molecules are coupled in an orientation that does not allow an interaction with the redox partners. These randomly distributed Adx molecules do not contribute to the observed interaction curves and therefore do not influence the binding parameters. Adx or mutants were immobilized on a cell of the activated surface with a flow of 5 μL min^{-1} at 15 °C. Specific surfaces were obtained by injecting and coupling 50 μM Adx or Adx mutants diluted in Biacore HBS-EP buffer. CK2 phosphorylated Adx was coupled onto the activated dextran matrix by injecting a phosphorylation reaction mixture (see above for phosphorylation reaction) containing approximately 45 μM phosphorylated Adx. The immobilization procedure was completed by injecting 1 M ethanolamine hydrochloride in order to block the remaining ester groups. Approximately 200 RU (response units) of each Adx species were immobilized on the dextran matrix. Binding of AdR or CYP11A1 was analyzed after injecting solutions of the respective proteins with varying concentrations between 50 nM to 500 nM in HBS-EP buffer. Each concentration was injected at least three times. To visualize unspecific background interactions between the dextran matrix and the ligands (AdR or CYP11A1), reference cells were created. The dextran matrix of these cells was activated as described above. Afterward, the activated carboxyl groups were immediately capped with ethanolamine without coupling of Adx. After injection of the ligand, specific binding curves were obtained by subtracting the signal response of the reference cells from the signal obtained from cells containing coupled Adx.

To remove the bound AdR or CYP11A1, 10 μL of a 2 mM NaOH solution was injected. The regeneration performance was evaluated by analyzing the baseline response after up to 30 binding cycles with 500 nM CYP11A1 and 500 nM AdR. The observed changes were below 10%, indicating good regeneration. K_A values were determined using Biaeval 3.1. Averaged binding curves for the interaction between different Adx species and varying AdR or CYP11A1 concentrations were fitted simultaneously with a 1:1 binding model. K_A values were determined from the fit with the lowest standard deviation.

Kinetics by Rapid Mixing. Stopped-flow measurements were carried out with a single channel stopped-flow SX-17MV spectrophotometer equipped with PEEK tubings (Applied Photophysics) at 15 °C. Anaerobic conditions were achieved by incubation for 30 min with argon-bubbled buffer containing 5 mM dithionite followed by repeated flushing with excessively Ar-bubbled reaction buffer to remove oxygen from the system. All samples were prepared in a glovebox in an oxygen-free atmosphere. The reductions by AdR of Adx, the Adx mutants, and phosphorylated Adx were monitored by following the absorption decrease of Adx at 414 nm (absorption maximum of oxidized Adx or Adx mutants)[36,24] for 1.5 s, recording 4000 data points. The mutants Adx-T71E and Adx-T71V were used as positive and negative controls, respectively. AdR was reduced with NADPH in 20-fold excess, generating the reduced state of AdR throughout the measurement. After rapid mixing in the stopped-flow spectrophotometer, each sample contained 10 μM AdR, 200 μM NADPH, and varying Adx concentrations in the range from 0 to 20 μM. Reduction rates (k_{obsd} values) were determined by fitting the transient traces with a single-step reaction mechanism. Values were derived from six independent measurements.

To follow the reduction of cytochrome CYP11A1 by AdR-reduced Adx, the absorption changes were monitored at 450 nm, which corresponds to the formation of the ferrous−carbon monoxide complex.[37−40] Prior to mixing, syringe A contained CYP11A1 (2 μM) while syringe B was filled with NADPH (200 μM), AdR (2 μM), and varying concentrations of the different Adx species in the range from 0.5 to 64 μM.

The mixture in syringe B was allowed to age for 5 min to ensure complete reduction of Adx. All proteins were diluted in a 50 mM HEPES buffer (pH 7.4) with 0.05% Tween 20. The solutions in the two syringes were saturated with CO prior to loading into the driving syringes. The reaction was monitored at 450 nm, recording 4000 data points, with a split time base of 10/100 s. The dead time for the measurements was 1.3 ms with the SX-17MV apparatus. All resulting curves were evaluated using SigmaPlot 2001. Kinetic traces were analyzed using monoexponential or biexponential fits to extract corresponding CYP11A1 reduction rates. Values shown in Figure 4 were derived from six independent measurements. The k_{obsd} values were plotted against the corresponding Adx concentration, and the curve was fitted with a hyperbolic equation in order to extract the concentration-independent reaction rate, k_{ET}. These plots were also used to obtain K_A

(29) Studier, F. W. *J. Mol. Biol.* **1991**, *219*, 37−44.
(30) Uhlmann, H.; Beckert, V.; Schwarz, D.; Bernhardt, R. *Biochem. Biophys. Res. Commun.* **1992**, *188*, 1131−1138.
(31) Sagara, Y.; Wada, A.; Takata, Y.; Waterman, M. R.; Sekimizu, K.; Horiuchi, T. *Biol. Pharm. Bull.* **1993**, *16*, 627−630.
(32) Kimura, T. In *Structure and Bonding*; Jorgensen, C. K., Neilands, J. B., Nyholm, R. S., Reinen, D., Williams, R. J. P., Eds.; Springer-Verlag: Berlin, 1968; Vol. 5, pp 1−40.
(33) Hiwatashi, A.; Ichikawa, Y.; Maruya, N.; Yamano, T.; Aki, K. *Biochemistry* **1976**, *15*, 3082−3090.
(34) Akhrem, A. A.; Lapko, V. N.; Lapko, A. G.; Shkumatov, V. M.; Chashchin, V. L. *Acta Biol. Med. Ger.* **1979**, *38*, 257−273.
(35) Faust, M.; Schuster, N.; Montenarh, M. *FEBS Lett.* **1999**, *462*, 51−56.
(36) Schiffler, B.; Zollner, A.; Bernhardt, R. *J. Biol. Chem.* **2004**, *279*, 34269−34276.
(37) Schiffler, B.; Kiefer, M.; Wilken, A.; Hannemann, F.; Adolph, H. W.; Bernhardt, R. *J. Biol. Chem.* **2001**, *276*, 36225−36232.
(38) Lange, R.; Heiberlanger, I.; Bonfils, C.; Fabre, I.; Negishi, M.; Balny, C. *Biophys. J.* **1994**, *66* (1), 89−98.
(39) Tuckey, R. C.; Kamin, H. *J. Biol. Chem.* **1983**, *258* (7), 4232−4237.
(40) Kashem, M. A.; Lambeir, A. M.; Dunford, H. B. *Biochim. Biophys. Acta* **1987**, *911* (2), 162−167.

values for the interaction between the relevant redox states of the reacting proteins.

Stopped-flow experiments with varying ionic strength were also performed. The reaction buffer consisted of 50 mM HEPES (pH 7.4), varying amounts of potassium chloride, and 0.05% Tween 20. The pH of the buffer was measured after salt addition and remained constant. After mixing, the samples contained 1 μM CYP11A1, 1 μM AdR, 1 μM Adx, and 100 μM NADPH.

Computational Methods

Preparation of Structures for Simulations. The crystallographic structure of Adx was obtained from Protein Data Bank entry 1CJE.[41] Chain B was selected from the crystal structure, which contains amino acids 5−111. The C-terminal carboxyl group was added to Val-111 using Sybyl 6.5.[42] The hydrogens were added using NAMD,[43] and in order to relax the structural strain from the crystal structure, the structure was equilibrated using water in a box that extends 7 Å beyond each dimension of the protein with an ionic strength of 50 mM as the solvent. The Charmm27 force field[44] was used. For the first 150 ps of the equilibration, velocity reassigning and strong constraints were assigned and then an additional 400 ps equilibration with no constraints. The simulations were performed at constant temperature and pressure by setting the Langevin thermostat and the Langevin piston temperatures to 310 K. Three additional structures were created by mutating residue 71 of the equilibrated Adx structure to valine, glutamic acid, and phosphorylated threonine, respectively, using Sybyl 6.5, and then each structure was energy minimized within a 3.0 Å radius of the mutation using the conjugate gradient method and the Tripos force field. Since phosphorylation can affect the protein conformation and hydrogen bond network, the phosphorylated structure was equilibrated for 800 ps at constant temperature and pressure via Langevin dynamics. The CHARMM27 force field was modified to include parameters for the iron−sulfur cluster[52] and the phosphate group. The phosphate parameters were based on those for dimethylphosphate in the Charmm22 force field.

A homology model, generously provided by J. A. Peterson and S. Graham, was used for CYP11A1.[45] The steric conflict between the heme cofactor and Arg420 was removed by performing a modest energy minimization of the affected area using Sybyl 6.5. Hydrogens were added using the program REDUCE,[46] which also determined the appropriate protonation state for each His.

PATHWAY coupling maps for each structure were calculated using HARLEM[47] and all nonpolar hydrogens were removed for the BD simulations.

Brownian Dynamics Simulations. We modified the program Simulation of Diffusional Association (SDA)[48] to perform BD simulations of the interaction and ET kinetics between Adx and CYP11A1. The SDA program itself only simulates diffusion-controlled kinetics of protein−protein interactions. We modified the code so that it can simulate both diffusion-controlled and ET-controlled mechanisms using an adaptation of the methodology devised by Northrup et al.[49] The protein-mediated tunneling was described with the PATHWAYS[11] model.

All electrostatic calculations were performed with the UHBD[50] program. Partial atomic charges were set according to the AMBER94 united atom force field,[51] which was modified to include partial charges for the iron−sulfur cluster and its cysteine ligands using values from DFT calculations,[52] as well as parameters for the phosphate group that were based on those for dimethylphosphate in the CHARMM22 force field. Grid dimensions of 150 × 150 × 150 Å^3 were used with 1.0 Å grid spacing and were centered on each protein. The dielectric constants of the protein and solvent were set to 4 and 78, respectively. The ionic strength of the solvent was set to 50 mM to match experimental conditions.

The solvent was modeled as a continuum, and intermolecular forces and torques were represented by the sum of repulsion and electrostatic forces. Short-range repulsion forces were included by not allowing overlap of the exclusion volumes of the proteins, defined by monitoring the van der Waals overlap. Electrostatic forces were approximated from a sum of charge interaction terms calculated from the effective charges and a desolvation term.[53] The effective charges for each protein were fit to reproduce the electrostatic potentials derived from the UHBD calculations. These effective charges were placed on the carboxylate oxygen atoms of Asp, Glu, and the C-terminus; on the amine nitrogen atoms of Lys, Arg, and the N-terminus; on each atom of the [2Fe−2S] cluster; and on the Fe from the heme. A desolvation energy scaling factor[54] of 5.0 was determined by comparing the binding free energies calculated using the UHBD electrostatic calculations to those calculated using the effective charges.

Both CYP11A1 and Adx were treated as rotating rigid bodies in the simulations, and the translational motion was simulated for Adx relative to CYP11A1. The BD trajectories were begun with Adx randomly oriented 150 Å from CYP11A1, and a trajectory truncation distance was set to 500 Å. A variable time step was utilized with a time step of 0.5 ps when the proteins were less than 75 Å apart and then increased linearly with increasing intermolecular separation.[53] Four independent BD simulations were run with 5000 trajectories each, and each run contained enough reaction events to be statistically significant. The reaction event was defined using the ET reaction criteria, using the PATHWAYS model for ET.[11] The coupling value for each BD configuration was computed using[55]

$$|T_{DA}| \propto \mathrm{MAX}\{\epsilon_{inter} \prod_i \epsilon_i^D \prod_j \epsilon_i^A\} \quad (1)$$

where the products over $\epsilon^{D/A}$ values represent the strongest pathway from the cofactor to each surface atom on the Donor/Acceptor, and ϵ_{inter} represents the parameter describing the through-space decay from Adx to CYP11A1 from each surface atom on the respective proteins and is calculated by

$$\epsilon_{inter} = 0.6\, e^{-0.75(R-3.0)} \quad (2)$$

where R is the distance between the surface atoms on the respective

(41) Pikuleva, I. A.; Tesh, K.; Waterman, M. R.; Kim, Y. *Arch. Biochem. Biophys.* **2000**, *373*, 44−55.
(42) *SYBYL 6.5*; Tripos Inc., 1699 South Hanley Rd., St., Louis, Missouri, 63144, U.S.A.
(43) Kalé, L.; Skeel, R.; Bhandarkar, M.; Brunner, R.; Gursoy, A.; Krawetz, N.; Phillips, J.; Shinozaki, A.; Varadarajan, K.; Schulten, K. *J. Comput. Phys.* **1999**, *151*, 283−312.
(44) MacKerell, A. D., Jr., et al. *J. Phys. Chem. B* **1998**, *102*, 3586−3616.
(45) Usanov, S. A.; Graham, S. E.; Lepesheva, G. I.; Azeva, T. N.; Strushkevich, N. V.; Gilep, A. A.; Estabrook, R. W.; Peterson, J. A. *Biochemistry* **2002**, *41*, 8310−8320.
(46) Word, J. M.; Lovell, S. C.; LaBean, T. H.; Taylor, H. C.; Zalis, M. E.; Presley, B. K.; Richardson, J. S.; Richardson, D. C. *J. Mol. Biol.* **1999**, *285*, 1733−1747.
(47) Kurnikov, I. HARLEM; http://www.kurnikov.org/harlem_main.html.
(48) Gabdoulline, R. R.; Wade, R. C. *Methods* **1998**, *14*, 329−341.
(49) (a) Andrew, S. M.; Thomasson, K. A.; Northrup, S. H. *J. Am. Chem. Soc.* **1993**, *115*, 5516−5521. (b) Northrup, S. H.; Allison, S. A.; McCammon, J. A. *J. Chem. Phys.* **1984**, *80*, 1517−1524. (c) Eltis, L. D.; Herbert, R. G.; Barker, P. D.; Mauk, A. G.; Northrup, S. H. *Biochemistry* **1991**, *30*, 3663−3674. (d) Madura, J. D.; Davis, M. E.; Gilson, M. K.; Wade, R. C.; Luty, B. A.; McCammon, J. A. *Rev. Comput. Chem.* **1994**, *5*, 29−267.
(50) Madura, J. D.; Briggs, J. M.; Wade, R. C.; Davis, M. E.; Luty, B. A.; Ilin, A.; Antosiewicz, J.; Gilson, M. K.; Bagheri, B.; Scott, L. R.; McCammon, J. A. *Comput. Phys. Commun.* **1995**, *91*, 57−95.
(51) Cornell, W. D.; Cieplak, P.; Bayly, C. I.; Gould, I. R.; Merz, K. M.; Ferguson, D. M.; Spellmeyer, D. C.; Fox, T.; Caldwell, J. W.; Kollman, P. A. *J. Am. Chem. Soc.* **1995**, *117*, 5179−5197.
(52) Noodleman, L.; Peng, C. Y.; Case, D. A.; Mouesca, J. M. *Coord. Chem. Rev.* **1995**, *144*, 199−244.
(53) Gabdoulline, R. R.; Wade, R. C. *J. Phys. Chem.* **1996**, *100*, 3868−3878.
(54) (a) Gabdoulline, R. R.; Wade, R. C. *J. Mol. Biol.* **2001**, *306*, 1139−1155. (b) Elcock, A. H.; Gabdoulline, R. R.; Wade, R. C.; McCammon, J. A. *J. Mol. Biol.* **1999**, *291*, 149−162.
(55) Beratan, D. N.; Betts, J. N.; Onuchic, J. N. *Science* **1991**, *252*, 1285−1288.

Table 1. Kinetic and Thermodynamic Parameters of Different Adx Species Interacting with Their Redox Partners, AdR and CYP11A1

Adx species	K_A[a] (Adx_{ox} + AdR_{ox}) $[M^{-1}] \times 10^6$	K_A[a] (Adx_{ox} + $CYP11A1_{ox}$) $[M^{-1}] \times 10^6$	K_A[b] (Adx_{ox} + AdR_{red}) $[M^{-1}] \times 10^6$	K_A[b] (AdR_{red} + $CYP11A1_{ox}$) $[M^{-1}] \times 10^6$	$k_{obsd,max}$[b] (Adx by AdR) $[s^{-1}]$	$k_{obsd,max}$[b] (Adx-dependent CYP11A1–CO complex formation) $[s^{-1}]$	$k_2 = K_A k_{obsd,max}$ (Adx + CYP11A1) $[M^{-1} s^{-1}] \times 10^6$	k_2(simulated)[d] (Adx + CYP11A1) $[M^{-1} s^{-1}] \times 10^6$
WT	1.16	74.6	0.36 ± 0.03	0.35 ± 0.05	7.75 ± 0.15	3.07 ± 0.10	1.1	19 ± 7
T71V	1.26	60.7	0.35 ± 0.04	0.33 ± 0.03	7.97 ± 0.24	3.19 ± 0.20	1.0	10 ± 4
T71E	1.19	132.0	0.32 ± 0.05	0.56 ± 0.08	7.70 ± 0.23	3.68 ± 0.11	2.1	57 ± 2
phosphorylated	1.20	112.0	0.39 ± 0.08	0.60 ± 0.07[c] 0.37 ± 0.08[c]	7.62 ± 0.42	46.68 ± 3.23[c] 3.66 ± 0.27[c]	28.0[c] 1.4[c]	650 ± 20

[a] Values obtained from optical biosensor analysis with approximately 200 RU of each Adx species covalently coupled to the sensor chip using an EDC/NHS solution. Averaged interaction curves were fitted simultaneously using a 1:1 binding model, and association constants ($K_A = k_{on}/k_{off}$) were determined using Biaeval 3.1. The standard deviation is ±10% of the displayed value. [b] The reduction of Adx or mutants by AdR was followed at 414 nm in a stopped-flow assay. Kinetic traces were evaluated using monoexponential fits. The Adx-dependent formation of the CYP11A1−CO complex was measured at 450 nm in a stopped-flow assay. The transients were evaluated using monoexponential or biexponential equations. Overall maximal reaction rates were determined by fitting the plots shown in Figures 2 and 4 with a hyperbolic fit. K_D values extracted from these plots were converted to K_A values (K_A=1/K_D). [c] For phosphorylated Adx, the values were calculated from the fast and slow phases, respectively. [d] Values calculated from a Brownian dynamics simulation.

proteins. The value of 0.75 was chosen for the coupling element decay parameter (β/2) in order to represent the rate of tunneling through unstructured water.[56] The ET rate for each BD protein configuration was calculated using the nonadiabatic electron-transfer rate expression.[10] The value for the driving force, ΔG, was calculated to be 0.9 eV from the experimental redox potential values.[57] The reorganization energy, λ, was determined from the nonadiabatic rate expression by first running the simulations with a simple exponential distance model where $k_{ET} = k_0 \exp(-\beta r)$ using a range of values for β and k_0 in order to extract the electronic coupling value. The parameter combination that best correlated with experimental measurements of the ET rate was then used to estimate λ at 0.5 eV. This value is typical of interprotein reorganization energies,[58] although plausible values span a wide range.[2,6] Given the uncertainty of the reaction driving force, we have not attempted to fine-tune this parameter. The qualitative conclusions of the paper do not change with variation in λ, although the theoretical values reported in Table 1 do depend on this choice.

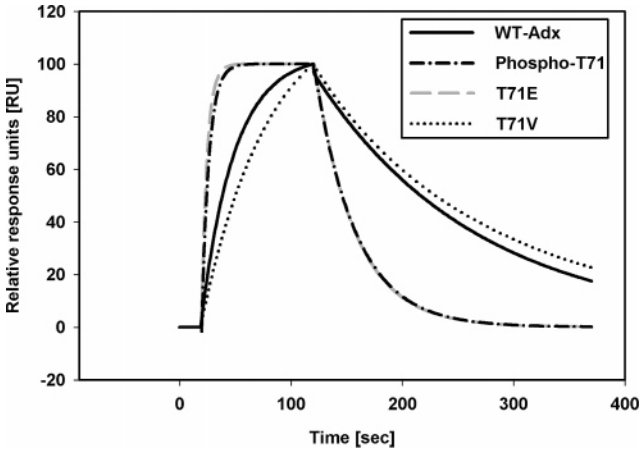

Figure 1. Normalized binding curves for the interaction between different oxidized Adx species and 100 nM CYP11A1 as measured with the optical biosensor technique (Biacore 2000).

Results

Functional Characterization of the Interaction between Adx and Its Redox Partners. To analyze the effects of a phosphorylation of residue T71 in mature Adx in vitro, we synthesized a mutant that simulates permanent phoshorylation at this position, Adx-T71E. The mutant is a convenient model for the phosphorylated protein because the phosphate group can be hydrolyzed (e.g., by phosphatase reactions or temperature jumps during purification). Substitution of Thr by Glu is widely used to simulate phosphorylation.[59] Additional experiments were performed with the phoshorylated Adx in order to compare its kinetics with that of the Adx-T71E mutant. Luciferase assays were used to estimate that the degree of phosphorylation of the mixture was always higher than 85% (results not shown.) In addition, a mutant that simulates a permanent unphosphorylated state, Adx-T71V, was used as a negative control.

Analysis of the binding behavior of the oxidized T71 mutants and CK2 phosphorylated Adx with AdR_{ox} and $CYP11A1_{ox}$ was performed via optical biosensor experiments. These experiments serve as a fast screening method for the direct visualization of changes in the binding of different Adx species with their redox partners, as has been examined in previous studies.[24,36] Binding parameters obtained for the interaction between WT-Adx and its redox partners are in the range of previously published data.[36,60] The results of these experiments appear in Table 1. Association constants for the interaction between AdR and the different Adx species were not changed compared with WT-Adx. Figure 1 shows the binding curves for the interaction between different Adx species and CYP11A1. The association constants (K_A) for the interaction between CYP11A1 and Adx-T71E or phosphorylated Adx were about 1.5-fold increased compared to the WT protein. The negative control, Adx-T71V, displays a similar binding constant with CYP11A1 as does Adx-WT. This data indicate that only the binding with CYP11A1 was slightly altered by the introduction of additional negative charges at residue T71, whereas the interaction with AdR was not affected.

Since the data from the Biacore experiments (Table 1) and results that were recently published from in vitro reconstitution assays[1] reveal changes in the interactions between the different Adx species and their redox partners, it is interesting to speculate that the ET kinetics might also be impacted. Stopped-flow kinetic measurements were used to analyze the influence of the

(56) Ponce, A.; Gray, H. B.; Winkler, J. R. *J. Am. Chem. Soc.* **2000**, *122*, 8187−8191.
(57) Lambeth, J. D.; Seybert, D. W.; Kamin, H. *J. Biol. Chem.* **1980**, *255*, 138−143.
(58) Miyashita, O.; Okamura, M. Y.; Onuchic, J. N. *J. Phys. Chem. B* **2003**, *107*, 1230−1241.
(59) Zhao, Y.; Hawes, J.; Popov, K. M.; Jaskiewicz, J.; Shimomura, Y.; Crabb, D. W.; Harris, R. A. *J. Biol. Chem.* **1994**, *269*, 18583−18587.
(60) Ivanov, Y. D.; Usanov, S. A.; Archakov, A. I. *Biochem. Mol. Biol. Int.* **1999**, *47*, 327−336.

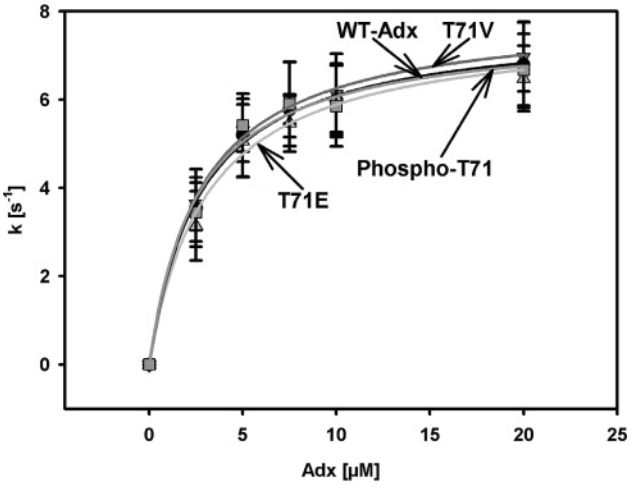

Figure 2. Observed rate constants for the reduction of Adx by NADPH prereduced AdR as a function of the concentration of Adx as measured by stopped-flow analysis. Data points represent averaged values determined from six independent measurements, with error bars representing the standard deviations. Hyperbolic fits were used to analyze the plots. All samples contained 10 μM AdR, 200 μM NADPH, and varying concentrations of Adx (0−20 μM) in 50 mM HEPES, pH 7.4 with 0.05% Tween20.

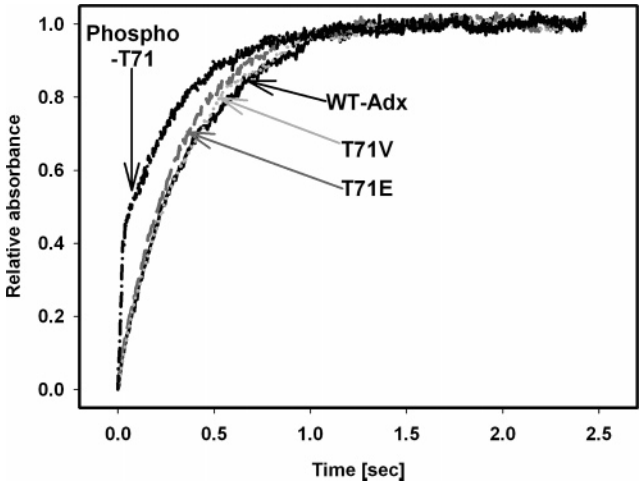

Figure 3. Stopped-flow analysis of the reduction of CYP11A1 monitored at 450 nm using different Adx species. Curves were obtained for the different Adx species, and the mono- or biexponential fit are in the Supporting Information. The transient curves recorded for the reduction of CYP11A1 by phosphorylated Adx were always best described by a biexponential process, while all other Adx species could be fit to a single-exponential reaction mechanism. All displayed samples contained 1 μM CYP11A1, 1 μM AdR, 8 μM Adx, and 100 μM NADPH. Reactions were performed in 50 mM HEPES, pH 7.4 with 0.05% Tween20 at 15 °C.

charge insertions at position T71 of Adx on the electron-transfer kinetics. Additionally, these experiments served to determine whether the association constant for the interaction between the relevant redox states of the reacting proteins, i.e., Adx_{ox} and AdR_{red} or Adx_{red} and $CYP11A1_{ox}$, has also been affected by the charge insertion at residue T71 as shown for the oxidized proteins (Figure 1).

Analysis of the reduction of Adx by prereduced AdR was investigated by following the absorption decrease at 414 nm and revealed no changes between the different Adx species (data not shown). Figure 2 shows the Adx concentration dependency upon reduction by AdR. The rate and binding constants extracted from these plots are given in Table 1. The differences between the association constants determined using the optical biosensor measurements and the stopped-flow methodology can be attributed to redox potential shifts of Adx upon reduction (−274 mV to −360 mV)[61] as well as to an enhanced flexibility of the loop surrounding the iron−sulfur cluster in Adx,[62,63] both being factors that favor the complex dissociation. However, as seen in Table 1, the association constants determined for the different Adx-T71 species are (independent of the technique used) almost identical, suggesting no relevant changes in the interaction between these redox partners. Additionally, the maximal reaction velocities in Table 1 that were extracted from the plots in Figure 2 show that electron transfer from reduced AdR to Adx has also not been significantly altered by the charge insertion at residue T71.

The reduction rate of heme-containing CYP11A1 was estimated by measuring the velocity of the CYP11A1−CO complex formation at 450 nm. This complex is formed after cytochrome reduction.[27,36] Binding of CO to the reduced heme iron of CYP11A1 can be considered irreversible. Previous stopped-flow experiments[38,39,40] estimated the association rate for the CYP11A1−CO complex formation to be approximately 2.3 × 10^5 M^{-1} s^{-1} and a significantly slower dissociation velocity (approximately 0.06 s^{-1}). Considering a simple one-step model for the CYP11A1−CO complex formation, k_{obsd} is defined as $k_{obsd} = K_a[CO] + K_d$. As applied in this study, the concentration of CO in a saturated solution at 15 °C and under atmospheric pressure is approximately 1 mM, so k_{obsd} for the CYP11A1−CO complex formation is approximately 230 s^{-1}. This observed reaction rate is significantly faster by over 2 orders of magnitude than the k_{obsd} values obtained for the reduction of CYP11A1 by Adx. Therefore, the CYP11A1−CO complex formation is expected to have a negligible effect on the observed rate for the reduction of CYP11A1 by Adx using stopped-flow techniques.

The saturation kinetics for this reaction between reduced Adx and oxidized CYP11A1 was studied in order to correlate the observed reduction rates with the ET rate; the maximal observed velocity ($k_{obsd,max}$) is equivalent to k_{ET}. The dependence of the Adx concentration on the saturation kinetics was also measured.

Figure 3 shows representative time-dependent absorption curves obtained from the stopped-flow experiments for all Adx species. Only phosphorylated Adx displays biexponential behavior, whereas all other Adx species exhibited monoexponential behavior (see Supporting Information). The kinetic trace obtained for the phosphorylated Adx is characterized by a fast first dominant phase (60% of the total amplitude change) that is followed by a second slower phase. The results of concentration-dependent, stopped-flow experiments are given in Figure 4. All Adx species reach saturation at a concentration of approximately 16 μM Adx, including both phases of the phosphorylated Adx sample. In addition, WT-Adx, Adx-T71V, and Adx-T71E all still only display monoexponential behavior at higher Adx concentrations. Table 1 shows the reduction rates extracted from hyperbolic fits of these curves; the value determined for the WT-Adx dependent CYP11A1−CO complex formation is comparable to recently published data.[36] For the negative control, Adx-T71V, the maximal measured reduction rate for the monoexponetial CYP11A1−CO complex formation

(61) Lambeth, J. D.; Seybert, D. W.; Lancaster, J. R., Jr.; Salerno, J. C.; Kamin, H. *Mol. Cell Biochem.* **1982**, *45*, 13−31.
(62) Kostic, M.; Bernhardt, R.; Pochapsky, T. C. *Biochemistry* **2003**, *42*, 8171−8182.
(63) Shakya, S. K.; Gu, W.; Helms, V. *Biopolymers* **2005**, *78*, 9−20.

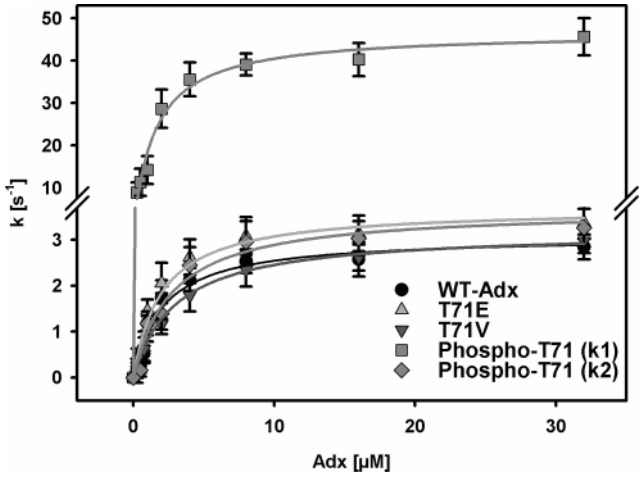

Figure 4. Adx concentration-dependent, stopped-flow analysis of the kinetics of various Adx species with CYP11A1. Reactions were performed in 50 mM HEPES, pH 7.4 with 0.05% Tween20. The velocity for formation of the CYP11A1−CO complex, which depends upon the reduction of the cytochrome by Adx, was determined via exponential fits to the data. The samples contained 1 μM CYP11A1, 1 μM AdR, and 100 μM NADPH.

is 3.19 s^{-1}, which is practically equivalent to the reduction rate of WT-Adx. A slightly increased, reproducible value of 3.68 s^{-1} is obtained for the mutant that mimics phosphorylation, Adx-T71E. For phosphorylated Adx, the second slower phase is in the range of the monoexponentially determined reduction rates for the other Adx species, but the first fast phase is increased approximately 12-fold ($k_{obsd,max,1} = 46.7\ s^{-1}$).

Radioactive labeling of Adx using $^{33}P\gamma ATP$ showed that the phosphate group is stably inserted into the Adx molecule for at least 1 h.[1] Since the relatively fast kinetic reaction takes place within seconds, the phosphate group is not likely to be cleaved off before or during the reaction and hence be the cause of the second phase (also in the seconds regime) that is observed in the kinetic traces for phosphorylated Adx. In addition, the degree of phosphorylation was measured via a luciferase assay prior to each experiment as described in the methods section. The degree of phosphorylation was always between 85 and 90% (results not shown) and is comparable to previous studies,[1] indicating a high phosphorylation rate of Adx by CK2. It is possible that part of the slower second phase observed in the stopped-flow measurement is caused by the 10−15% of the sample that contains unphosporylated Adx, since the obtained reaction velocity for the second phase is in the range of the value obtained for WT-Adx. However, this small percentage of unphosphorylated Adx present in the sample is not likely to be the only cause for the observed 40% amplitude change of the second phase. Moreover, the main changes of this second phase can be attributed to the phosphorylated species from the concentration-dependent, stopped-flow experiments in Figure 4. This biphasic behavior could be an artifact, which is unlikely since the biexponential behavior was also visible when using different concentrations of the phosphorylated species, and both phases displayed a saturation behavior that is concentration dependent. If the second phase was an artifact, both observed velocity rates would not be expected to reach the same maximal velocity when using different concentrations of the phosphorylated species. Since the experimental setup using all Adx species was always the same and the two phases were only visible using the phosphorylated species, the biexponential behavior can be clearly attributed to the phosphorylated species.

The observed differences between the association rates determined for the Adx−AdR interaction using the optical biosensor technique and the stopped-flow methodology appear to be caused by the different oxidation states of the proteins depending on the method used. For the interaction between AdR and Adx, both methods indicate that the binding constants of the two Adx species containing an additional charge at position T71, Adx T71E and phosphorylated Adx, were enhanced (approximately 1.5-fold) compared to the wild type. The association rates extracted from the stopped-flow measurements that reflect the interaction between the relevant redox states of the proteins allowed the determination of K_A values for both phases of the reduction of CYP11A1 by phosphorylated Adx. The K_A value of the first fast predominant phase was greater than the K_A value for the second phase (2-fold increased), indicating an increase in binding.

Additional stopped-flow experiments performed with varying ionic strength indicate that the interactions between all Adx species and CYP11A1 depend on electrostatic interactions. These measurements revealed a pronounced decrease in the observed CYP11A1 reduction rates at higher ionic strength for all Adx species (data not shown). This observation is consistent with the ionic nature of the complex between Adx and CYP11A1.[64−68]

BD Simulations. The results of the structural refinements of Adx using NAMD[43] and Sybyl6.5[42] are given in Figure 5a. The most pronounced structural change occurs in the phosphorylated structure (in red), particularly near the phosphate group at residue 71 and the α helix that comprises a large part of the interaction region with its redox partners, residues 72−79. Additionally, there is a small shift in the position of the iron−sulfur cluster. These structures are colored in Figure 5b according to their electronic coupling values obtained from a PATHWAYS calculation. The electronic coupling values for the protein backbone are not significantly altered by the slight structural deviations. However, for the mutated residue 71, both the phosphate and the glutamic acid mutations have atoms that have higher coupling magnitudes than those of the corresponding valine mutation or the threonine from the original crystal structure. The bimolecular rates calculated from the BD simulations are given in Table 1 together with the rate constants calculated from the stopped-flow measurements. The values that were calculated from experimental measurements assume that the kinetics are ET-controlled, so the bimolecular rate is the product of the electron-transfer rate and the binding affinity averaged over each binding geometry. The bimolecular rates from the simulations are an order of magnitude larger than those from experiments but reproduce the observed kinetic trends.

The differences in the measured values and the simulated rate constants could indicate that the reaction might exhibit a conformational gating, which would require a rearrangement of the complex prior to the electron-transfer event to take place.

(64) Lambeth, J. D.; Geren, L. M.; Millett, F. *J. Biol. Chem.* **1984**, *259*, 10025−10029.
(65) Tuls, J.; Geren, L.; Lambeth, J. D.; Millett, F. *J. Biol. Chem.* **1987**, *262*, 10020−10025.
(66) Adamovich, T. B.; Pikuleva, I. A.; Chashchin, V. L.; Usanov, S. A. *Biochim. Biophys. Acta* **1989**, *996*, 247−253.
(67) Tuls, J.; Geren, L.; Millett, F. *J. Biol. Chem.* **1989**, *264*, 16421−16425.
(68) Wada, A.; Waterman, M. R. *J. Biol. Chem.* **1992**, *267*, 22877−22882.

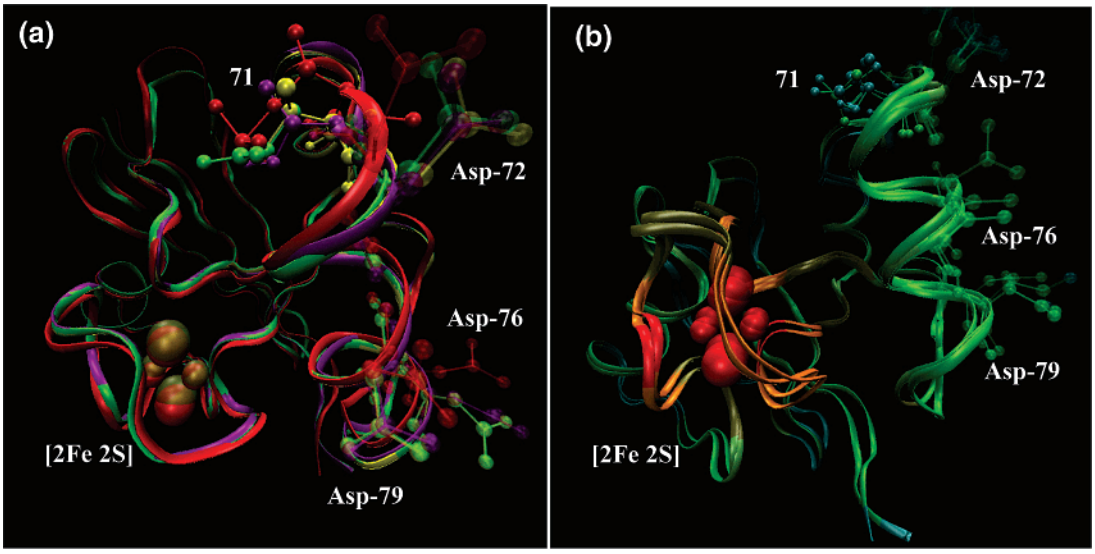

Figure 5. Overlay of Adx protein structures that were prepared for the BD simulations. (a) The crystal structure is in purple, Adx-T71V is yellow, Adx-T71E is green, and phosphorylated Adx is red. The iron−sulfur cluster and Asp residues that are important for interactions with its redox partners are indicated, as well as residue 71, which is the site of mutations. (b) Same structures as those in (a), except each structure is colored according to its electronic coupling values. The electronic coupling values were calculated with the PATHWAYS analysis in HARLEM.[47] Red indicates the strongest coupling, and blue indicates the weakest. The images were created using VMD.[69]

Therefore, the k_{obsd} value would include an equilibrium constant for this rearrangement reaction resulting in the following equation: $k_{obsd} = K_{eq}\, k_{ET}$. Comparison of the simulated k_2 values with the experimentally obtained values suggests the K_{eq} value for this process to be approximately 0.1. Since BD simulations do not describe such complex rearrangements, conformational gating could provide an explanation for the observed small differences in the k_2 values obtained from the experimental and theoretical approach. However, such possible rearrangements of the $CYP11A1_{ox}-Adx_{red}$ have not been investigated so far.

The k_2 values determined for the different Adx species showed that the Adx-T71V mutation produced a slightly lower k_2 rate than that in the wild type, and the Adx-T71E mutation produced a slightly higher k_2 rate, which indicates a small increase in k_{ET}. This slightly increased k_{ET} value correlates perfectly well with the recently published results of in vitro and in vivo CYP11A1 substrate conversion assays.[1] For the phosphorylated structure, the k_2 from the BD simulations is an order of magnitude larger than the wild-type rate and correlates with the rate for the fast first phase in the biphasic reduction of CYP11A1 by phosphorylated Adx.

Figure 6 shows the mean residence time in the Brownian dynamics calculations for each Adx structure calculated per 1 Å slab of the interaction region with CYP11A1. Adx-T71E and phosphorylated Adx spend over twice the amount of time close to CYP11A1 than do either the WT or Adx-T71V, which is consistent with the optical biosensor and stopped-flow measurements. Since both Adx-T71E and the phosphorylated Adx are more negatively charged than WT and Adx-T71V, the increase in mean residence times suggests a correlation with complementary electrostatic interactions.

Figure 7 shows the center of mass of Adx as it interacts with CYP11A1 during a single BD trajectory, and only those configurations that are relevant to electron transfer (those with non-negligible electronic coupling) are indicated. The WT structure preferentially binds to two sites on P450 with essentially equal propensity, while the other Adx mutants favor

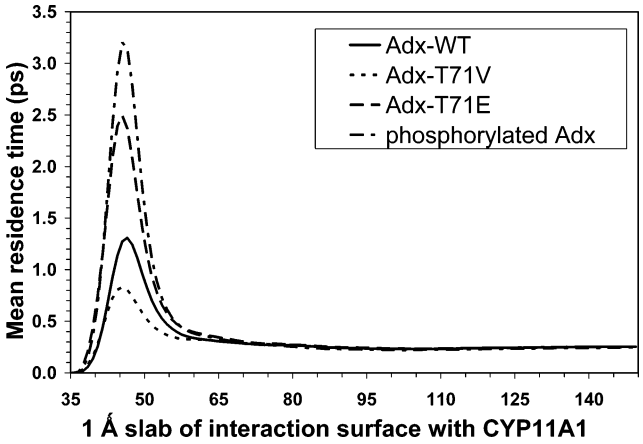

Figure 6. Mean residence time of each Adx species calculated per 1 Å slab of the interaction region with CYP11A1 from the Brownian dynamics calculations.

one site over the other. Both the Adx-T71V and Adx-T71E mutations preferentially associate with the region near residue Lys-405, where binding between Adx and CYP11A1 was found in previous docking.[45] However, the phosphorylated Adx type significantly prefers the region near Lys-193 and Phe-235.

Discussion

The role of post-translational modifications in electron-transfer reactions remains mostly obscure. Phosphorylation is known to alter the functionality of some proteins by inducing conformational changes.[70] Previous studies indicate that phosphorylation plays an active role in redox signaling that regulates energy transfer in chloroplasts,[71] thus providing an example of

(69) Humphrey, W.; Dalke, A.; Schulten, K. *J. Mol. Graphics* **1996**, *14*, 33−38.
(70) Komar-Panicucci, S.; Sherman, F.; McLendon, G. *Biochemistry* **1996**, *35*, 4878−4885.
(71) (a) Zhang, Z. L.; Huang, L. S.; Shulmeister, V. M.; Chi, Y. I.; Kim, K. K.; Hung, L. W.; Crofts, A. R.; Berry, E. A.; Kim, S. H. *Nature* **1998**, *392*, 677−684. (b) Vener, A. V.; Ohad, I.; Andersson, B. *Curr. Opin. Plant Biol.* **1998**, *1*, 217−223.

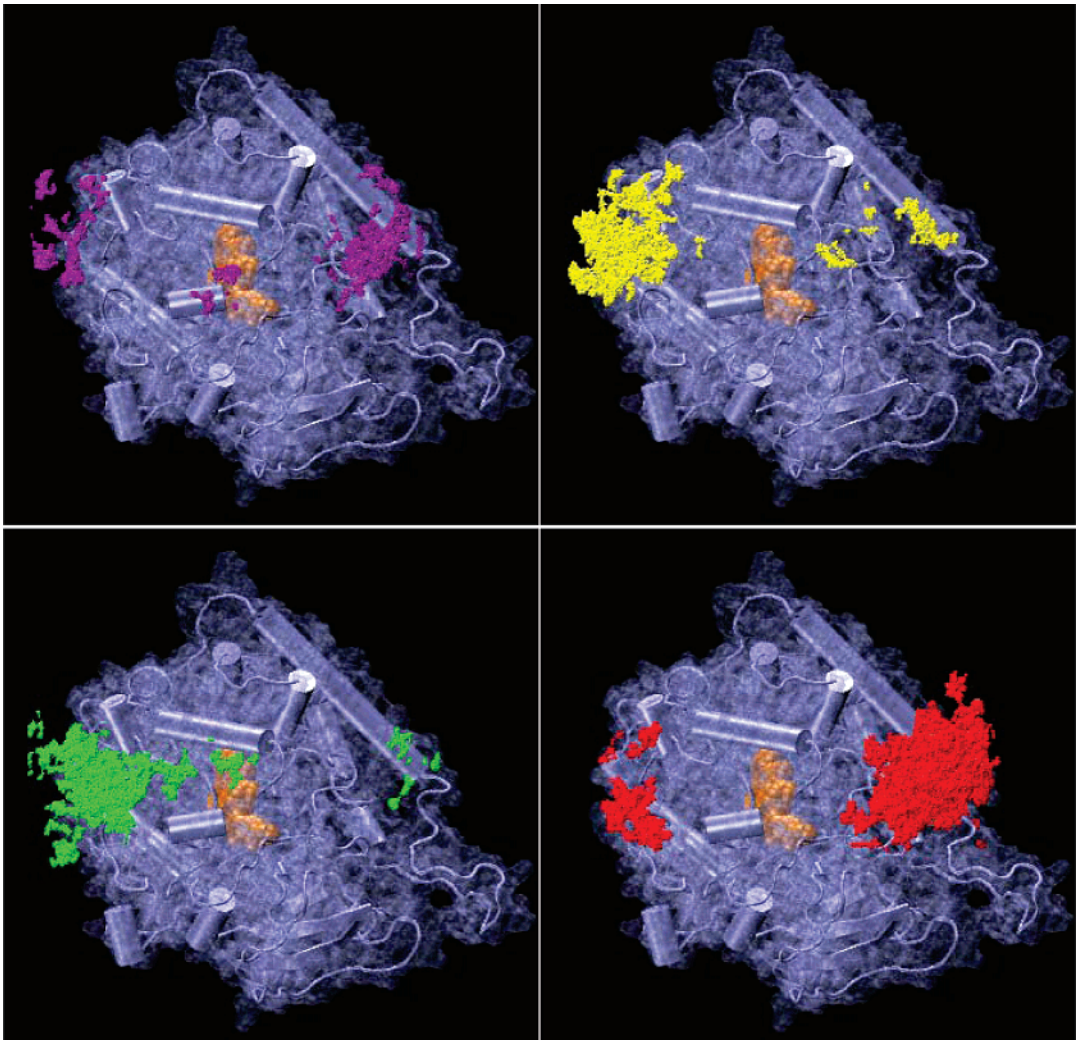

Figure 7. Structure of CYP11A1 overlaid with dots representing the center of mass of Adx from a single BD trajectory. Only conformations with non-negligible electronic coupling are shown. The Heme cofactor is shown in orange, wild-type Adx is in purple, Adx-T71V is yellow, Adx-T71E is green, and phosphorylated Adx is red. Lys-405 is to the left of the Heme cofactor, and Lys-193 is to the right. The images were created using VMD.[69]

signal transduction where electron-transfer reactions initiate phosphorylation and results in the regulation of the amount of harvested light by those organelles. The inverse process, namely the regulation of ET by phosphorylation, seems plausible. We have investigated the possible influences of phosphorylation on the adrenal mitochondrial steroid hydroxylating system. Here, electrons are being transferred from an NADPH-dependent reductase (AdR) to a [2Fe−2S] cluster ferredoxin (Adx) and then to a cytochrome P450 that catalyzes steroid hydroxylation.[22] The overall rate-limiting step in steroidogenesis is the formation of pregnenolone from cholesterol which is catalyzed by CYP11A1.[18b] The rate-limiting step in this electron-transfer chain, however, is the interaction between the ferredoxin and the cytochrome.[19,36] Therefore, it was of interest to analyze the influences of phosphorylation on the interaction between Adx and cytochrome $P450_{scc}$, CYP11A1.

Previous studies revealed that a homologous adrenodoxin protein from rat liver is phosphorylated by PKA[72,73] and that bovine Adx is the only component of the mitochondrial steroid hydroxylating system that can be readily phosphorylated by CK2, a ubiquitous and highly conserved Ser and Thr kinase.[1] The residue that is phosphorylated by this kinase, Thr-71, is located in the interaction domain of this ferredoxin that represents the primary region for redox partner recognition.[23,74] This primary interaction region is more flexible than the core domain of the protein, and this conformational flexibility may be relevant for the interaction of Adx with its redox partners. Therefore, phosphorylation of Thr-71 could alter its functionality.

Phosphorylation of T71 (or substitution of this Thr by Glu) increases the negative charge of the surface interaction region of Adx. Since the recognition between Adx and its redox partners is mainly based on electrostatic interactions and the dipole moment in Adx is considered to contribute to the docking kinetics of Adx and its redox partners,[22,75] additional negative charge could enhance complex formation. In the present studies, this hypothesis is confirmed by optical biosensor experiments as well as by the K_A values extracted from stopped-flow experiments. These experiments reproducibly (Table 1) indicate

(72) Siegel, N.; Wongsurawat, N.; Armbrecht, H. J. *J. Biol. Chem.* **1986**, *261*, 16998−17700.
(73) Nemani, R.; Ghazarian, J. G.; Moorthy, B.; Wongsurawat, N.; Strong, R.; Armbrecht, H. J. *J. Biol. Chem.* **1989**, *264*, 15361−15366.
(74) Vickery, L. E. *Steroids* **1997**, *62*, 124−127.
(75) Muller, A.; Muller, J. J.; Muller, Y. A.; Uhlmann, H.; Bernhardt, R.; Heinemann, U. *Structure* **1998**, *6*, 269−280.

an enhanced association constant toward CYP11A1 for Adx-T71E and phosphorylated Adx compared to WT-Adx, but there appears to be no effect on the association with AdR. Comparable results for interactions of Adx with CYP11A1 are obtained from the mean residence times extracted from BD simulations in Figure 6. The differential effect of these charge alterations at residue T71 on AdR and CYP11A1 association supports the idea that the binding sites on Adx for its interaction partners are overlapping rather than identical, as previously postulated.[22]

In the steady-state approximation for the donor−acceptor complex concentration, the pseudo-first-order ET rate is

$$k_1 = \frac{k_{on}k_{ET}[X]}{k_{off} + k_{ET} + k_{on}[X]} \quad (3)$$

when one reactant is present in excess.[76] In the saturation regime, the quasi-unimolecular rate is $k_1 = k_{ET}$, denoted $k_{obsd,max}$ in the tables, obtained by fitting the experimental data to eq 3. The bimolecular rate associated with interprotein ET (in the steady-state approximation) and when [X] is sufficiently small is

$$k_2 = \frac{k_{on}k_{ET}}{k_{off} + k_{ET}} \quad (4)$$

If ET is slower than complex dissociation, the bimolecular rate reaches the activation limit of $k_2 = K_A k_{ET}$, and when ET is fast, the reaction is diffusion limited, $k_2 = k_{on}$. The Brownian dynamics simulations have the ability to span the two mechanistic regimes without assuming either limiting behavior. Generalizations of this description that take explicit account of multiple donor−acceptor binding geometries appear in ref 15. The slowness of the kinetics measured here suggests activation limited kinetics.

Stopped-flow kinetic analysis (Table 1) shows a slightly enhanced (1.2-fold increase) CYP11A1 reduction rate with mutant Adx-T71E compared to WT, and the rate constants calculated from BD simulations produced the same trend. In contrast to all other Adx species, phosphorylated Adx displays biphasic reaction kinetics (Figures 3 and 4). These biexponential kinetics could indicate that reduced phosphorylated Adx is capable of binding to different regions of the cytochrome and that alternate ET pathways might be favored with the insertion of the phosphate group. Since the amplitude of the first rapid phase is greater (∼ 60%) than that of the second phase (∼ 40%), which also includes the reaction of the small percentage of unphosphorylated Adx present in the sample, the complex leading to faster ET kinetics could be thermodynamically favored over the conformation that resembles the complex conformation preferred by the other Adx species. The BD trajectory profiles in Figure 7 suggest that the phosphorylated Adx may preferentially associate with CYP11A1 in a different binding region than the WT-protein and the mutants, Adx-T71E and Adx-T71V. This secondary region on the CYP11A1 surface contains many polar and basic groups, which appear to attract the phosphate group and thus provide a more efficient electron-transfer pathway. By combining the information obtained from these docking profiles with the rate constants extracted from the stopped-flow experiments, it can be inferred that the slower second phase for the biexponential reduction of CYP11A1 by phosphorylated Adx corresponds to electron transfer at the binding site that WT-Adx, Adx-T71E, and Adx-T71V all seem to prefer, and the first fast phase corresponds to stronger binding to the additional electron-transfer site by the phosphorylated protein.

Of the two possible binding regions on the CYP11A1 surface, phosphorylated Adx appears to bind preferentially to the region near Lys-193, while all other species appear to bind preferentially to the region near residue Lys-405. As indicated by the biexponential stopped-flow kinetics, phosphorylated Adx is also capable of binding to the region near Lys-405 with an electron-transfer rate in the range observed for the other Adx species. Since the other Adx species seem to be capable as well of binding to the region around Lys-193, it may be postulated that the complex configuration involving Lys-193 may require a reorientation of the Adx species before ET is enabled, but that phosphorylated Adx may not require reorientation as has been proposed for other Adx species.[37] This assumption may provide an explanation for the observation that WT-Adx and the two Adx mutants preferentially bind to the region near residue Lys-405 and additionally provides an explanation for the biexponential behavior of the phosphorylated species. Since phosphorylated Adx displays biexponential electron-transfer kinetics, we suggest that the phosphorylation of T71 increases the efficiency of the electron-transfer pathway of this second complex configuration.

These studies also indicate that the substitution of a Thr residue by Glu does not fully simulate phosphorylation but rather approximates a permanent phosphorylated state. The differences observed for the phosphorylated Adx and the positive control, Adx-T71E, could be caused by minor structural changes indicated in Figure 5. In addition, a recent ^{31}P NMR study of the protonation state of *o*-phosphoserine showed that the pK_a value for the second proton of the phosphate is approximately 5.9,[77] so it can be hypothesized that phosphothreonine is also predominantly double deprotonated at pH 7.4. Therefore, a phosphorylation can introduce two additional negative charges and hence strengthen electrostatic interactions with the more basic region around Lys-193, whereas the substitution of Thr by Glu only introduces a single negative charge. This charge interaction could be involved in fine-tuning the orientation of phosphorylated Adx with CYP11A1 in this region. It is noteworthy that the mutant Adx-T71E exhibited a slightly increased ET rate and a significant increase in the binding affinity, indicating that this charge insertion enhances the ET in the region around Lys-405. The observation that both T71 mutants display differences in the docking profile compared to WT-Adx points toward an important role of the hydroxyl group of Thr-71 for the binding behavior of Adx toward CYP11A1. However, the fact that the mutant Adx-T71E preferentially associated with the region around residue Lys-405 indicates that the insertion of the phosphate group and hence two negative charges seems to facilitate the binding to the region around Lys-193, enabling a fast and efficient ET (which probably requires the above proposed fine-tuning mechanism). Moreover, the observed differences between the phosphorylated Adx and the T71E mutant could also be caused by the insertion of low-lying

(76) Bendall, D. S., Ed. *Protein Electron Transfer*; Bios Scientific Publishers, Oxford, UK, 1996.

(77) Gardiennet, C.; Henry, B.; Kuad, P.; Spiess, B.; Tekely, P. *Chem. Commun.* **2005**, 180−182.

phosphate orbitals that directly enhance donor−acceptor interactions as well as stabilize the complex of phosphorylated Adx with the region around residue Lys-193 of CYP11A1.

The results presented here raise the question of whether phosphorylation of Adx at position T71 is physiologically relevant or not. Recently published in vitro and in vivo data indicate that phosphorylation of Adx at Thr-71 leads only to an increase in the interaction with CYP11A1 and not with CYP11B1: the other natural interaction partner of Adx. CYP11A1 catalyzes the initial rate-limiting step of steroid biosynthesis, namely the side chain cleavage reaction that leads to the conversion of cholesterol to pregnenolone, which is the precursor molecule for all steroid hormones (for review, see ref 18b). Bovine CYP11B1, on the other hand, is involved in a series of hydroxylation reactions that result in the formation of cortisol and aldosterone, respectively (for review, see ref 20). A differentially altered interaction of phosphorylated Adx with CYP11A1 and CYP11B1, respectively, might suggest a regulatory function for phosphorylated Adx in steroidogenesis. However, it has not yet been possible to identify phosphorylated Adx unequivocally in cell culture experiments or directly in bovine tissue. It cannot be excluded that the phosphorylation of Adx at position T71 might only take place in certain developmental stages. For example, it has been suggested that phosphorylation of the microsomal cytochrome CYP17, which is involved in the synthesis of androgen sex steroids, is developmentally regulated.[78] Considering this, an enhancement of the CYP11A1-catalyzed formation of pregnenolone might be required. Since CYP11A1 competes with CYP11B1 for the common electron donor, a phosphorylation of Adx at residue Thr-71 could enhance the interaction with CYP11A1 and result in an increased production of the steroid precursor. Thus, phosphorylation might provide a fine-tuning mechanism that favors the formation of pregnenolone and the general steroid biosynthesis. Further in vivo experiments (e.g., primary cell culture experiments) may help to clarify the role of CK2 phosphorylation of Adx in steroidogenesis.

(78) Zhang, L. H.; Rodriguez, H.; Ohno, S.; Miller, W. L. *Proc. Natl. Acad. Sci. U.S.A.* **1995**, *92*, 10619−10623.

Conclusions

This study provides the first evidence that phosphorylation may play a role in the modulation of ET reactions. As indicated by both experimental and theoretical analysis, the phosphorylation seems to affect the binding geometries between Adx and CYP11A1 and may stabilize complex geometries that increase electron-transfer rates compared with WT-Adx. The Adx mutants investigated in this study, Adx T71E and Adx T71V, did not induce significant changes in the electron-transfer mechanism to CYP11A1. However, the mutant Adx T71E led to a slightly enhanced ET rate compared to WT-Adx. In addition, in combination with the results of a previously published study,[1] the data presented here point toward a potential role for phosphorylated Adx in fine-tuning the regulation of steroidogenesis. This putative regulatory role could be mediated by differences in the interaction between phosphorylated Adx with CYP11A1 and CYP11B1, respectively, which could lead to an increased formation of pregnenolone, the common steroidal precursor molecule. Taken together, these results indicate a possible role for CK2 in the regulation of steroidogenesis by primarily altering protein−protein interactions and by moderately affecting electron transfer.

Acknowledgment. We thank Wolfgang Reinle and Walter Klose for expert technical support, Rebecca Wade for providing the source code to the SDA program, Sandra Graham for providing the homology model for CYP11A1, Susanne Böhmer for proofreading the manuscript, the Volkswagen Stiftung (I/77 101) for generous financial support, the Fonds der Chemischen Industrie for grants to R.B., the NIH (GM-048043) for a grant to D.N.B., the Boehringer Ingelheim Fonds, and the Sloan Foundation for the postdoctoral fellowship awarded to M.A.P.

Supporting Information Available: Complete ref 44; mono- or biexponential fits for the transient curves from the stopped-flow analysis in Figure 3. This material is available free of charge via the Internet at http://pubs.acs.org.

JA064803J